Applied Catalysis B: Environmental 144 (2014) 66–74

Contents lists available at ScienceDirect

Applied Catalysis B: Environmental

journal homepage: www.elsevier.com/locate/apcatb

Understanding the influence of Ni, Co, Rh and Pd addition to PtSn/C catalyst for the oxidation of ethanol by in situ Fourier transform infrared spectroscopy

Seden Beyhan [a,b,*], Jean-Michel Léger [b], Figen Kadırgan [a]

[a] Department of Chemistry, Faculty of Science and Letters, Istanbul Technical University, 34469 Maslak, İstanbul, Turkey
[b] Electrocatalysis Group, IC2MP, UMR 7285, CNRS, Université de Poitiers, 40 avenue du Recteur Pineau, 86022 Poitiers Cedex, France

ARTICLE INFO

Article history:
Received 4 March 2013
Received in revised form 3 July 2013
Accepted 8 July 2013
Available online 17 July 2013

Keywords:
In situ infrared spectroscopy
Ethanol electrooxidation pathways
PtSn-based trimetallic catalyst

ABSTRACT

The reaction mechanism for the oxidation of ethanol on carbon supported Pt, PtSn and PtSn-based trimetallic catalysts has been investigated by in situ Fourier transform infrared (FTIR) spectroscopy. The results showed that the catalytic activity of $Pt_{80}Sn_{10}Ni_{10}/C$ and $Pt_{80}Sn_{10}Pd_{10}/C$ for electrooxidation of ethanol is directly favoured to acetic acid potential at around 0.25 and 0.3 V vs. RHE, respectively. These suggest that the addition of Ni or Pd to PtSn greatly enhances the formation of acetic acid at lower potential. However, Pt/C, $Pt_{80}Sn_{10}Ni_{10}/C$ and $Pt_{80}Sn_{10}Rh_{10}/C$ electrocatalysts showed a better performance than $Pt_{90}Sn_{10}/C$, $Pt_{80}Sn_{10}Co_{10}/C$ and $Pt_{80}Sn_{10}Pd_{10}/C$ electrocatalysts for the production of CO_2 during ethanol oxidation. Therefore, the pathway forming CO_2 is favoured by the presence of Ni and Rh in the PtSn.

1. Introduction

The electrooxidation of ethanol occurs by different reaction pathways [1–6]. In some pathways, partially oxidation products such as acetaldehyde and acetic acid or acetate [1,3–5] are produced which lead to decrease the total efficiency of the system. In other pathways, the formation of strongly adsorbed CO_{ads} species [3–5] and carbohydrate (CH_x) fragments [2,6] which poison the active sites on the Pt. A possible way to minimize the poisoning effect is to modify the composition of the electrode by adding second and/or third metals to the Pt surface. On the other hand, multi-metallic catalysts should cleave the C—C bond of the ethanol molecule to achieve total conversion at a low over potential.

Using in situ Fourier transform infrared (FTIR) spectroscopy and on-line Differential electrochemical mass spectrometry (DEMS) studies, Wang et al. [7] revealed that the addition of Sn or Ru to Pt does not enhance activity for C—C bond cleavage in ethanol. However, alloying Pt with Sn or Ru leads to lower the CO_{ad} surface coverage so the enhanced overall activity for ethanol oxidation. According to same authors, the yield of acetic acid on Pt/C, PtSn/C and PtRu/C catalysts increased with increasing electrode potential at the expense of acetaldehyde formation. Vigier et al. [8] reported that the addition of Sn to Pt/C catalyst favours the dissociative adsorption of ethanol and the formation of acetic acid compared to Pt at low potentials due to the bifunctional mechanism. On the other hand, the yield in CO_2 for Pt/C catalyst is two times higher than PtSn/C catalyst. This was explained that the need to have several adjacent platinum sites to adsorb ethanol molecule dissociatively and to break the C—C bond. Souza et al. [9] studied ethanol oxidation on electrodes of PtRh at different compositions by DEMS and FTIR spectroscopic techniques. According to their results, the acetaldehyde yield decreases when Rh added to the Pt electrode. However, CO_2 formation over acetaldehyde was improved on the electrodes $Pt_{73}Rh_{27}$ and $Pt_{55}Rh_{45}$ compared to Pt; the better selectivity was obtained by composition of (73:27). They concluded that Rh increases the ability for C—C bond cleavage in the ethanol; however, PtRh is not a good catalyst owing to decreasing overall rate of ethanol oxidation reaction.

Regarding the activity for the ethanol oxidation reaction, PtSn-based catalysts showed increased performance in comparison with PtRu-based catalysts [10]. Rousseau et al. [11] found that the addition of Ru to PtSn/C catalyst does not change the distribution products, however, the increased catalytic activity towards ethanol oxidation. Riberio et al. [12] were reported that the presence of Ir in the PtSn/C catalyst, prepared by Pechini–Adams modified method, may increase the catalyst roughness or structural defects which make the better catalytic activity than PtSn/C catalyst. Moreover, the increased surface oxophilicity owing to the Ir in the PtSn/C catalyst bring forth an increasing the Sn-O bond strength and the acidity of SnOH sites which favour the ethanol oxidation at lower

* Corresponding author at: Department of Chemistry, Faculty of Science and Letters, Istanbul Technical University, 34469 Maslak, Istanbul, Turkey.
Tel.: +90 212 285 72 70; fax: +90 212 285 63 86.
E-mail addresses: beyhanse@itu.edu.tr, seden1980@yahoo.com (S. Beyhan).

0926-3373/$ – see front matter © 2013 Elsevier B.V. All rights reserved.
http://dx.doi.org/10.1016/j.apcatb.2013.07.020

potentials. They also suggested that the presence of acetic acid is more important for Sn and Ir containing electrocatalysts which activate the interfacial water necessary for its formation the presence of small amount of adsorbed CO also indicated its easy removal of the surface of the catalysts through CO_2 formation. Zhu et al. [13] were prepared PtSnIn/C catalyst using $NaBH_4$ as a reducing agent in ethylene glycol solution and analyzed the anode products of the direct ethanol fuel cells at 0.5 V. They found that C_2 species are the major anode products which were similar to Rousseau's [11] results. Moreover, the yield of acetaldehyde on PtSnIn/C is much higher than that on PtSn/C. They proposed that the addition of In into PtSn/C catalyst leads to promotion of the α-H dissociation from ethanol which can enhance the performance of ethanol oxidation on the catalyst.

In this work, the influence of addition of the third metal element such as Ni, Co, Pd and Rh to PtSn/C catalyst for the ethanol oxidation reaction is investigated by in situ FTIR spectroscopy. The evaluation of the ethanol oxidation reaction product and selectivity of catalyst as a function of the applied potential is discussed, and possible ethanol oxidation pathways proposed.

2. Experimental

2.1. Preparation of electrodes

The preparation of the carbon supported Pt, bimetallic PtSn and trimetallic PtSnM (M = Ni, Co, Rh, Pd) catalysts is based on the procedure described by the Bönnemann method [14], but slightly modified as described in our previous papers [15,16]. Briefly, with the nominal composition of $Pt_{90}Sn_{10}$ and $Pt_{80}Sn_{10}M_{10}$ (M = Ni, Co, Rh, Pd) trimetallic colloidal nanoparticles were obtained by co-reduction of their corresponding non-hydrated metal chloride salts with the reducing agent $NOct_4$ [BEt_3H] in dry tetrahydrofurane (THF) under argon atmosphere. These highly dispersed colloidal nanoparticles were supported on a high surface area carbon (Vulcan XC72) with the metal loading of 40 wt.% through sonication until yielding a black waxy residue and then exposure to heat treatment in only nitrogen atmosphere at 300 °C for 1 h 30 min, which was differently than the original procedure, to generate activated carbon supported catalyst. After the heat treatment, the catalyst powder was washed several times with ethanol and distilled water and then dried overnight in a vacuum desiccator. Catalyst ink was prepared by dispersing of 25 mg of catalyst powder in a 2.5 ml of water solution containing 0.5 ml 5% Nafion® via sonication for 2 h. 8 μl of ink was pipetted onto a glassy carbon/gold disc working electrode (disc of 7 mm diameter) by micro syringe and dried at room temperature, which was polished with 0.5 μm alumina before each deposition to obtain the mirror-finished surface in order to obtain good reflectivity.

2.2. In situ FTIR spectroscopy measurements

A spectroelectrochemical cell fitted with a CaF_2 or ZnSe windows and a working electrode glued to a glass tube as the holder. The equipped cell with a calcium fluoride of (CaF_2) window is transparent to the incident beam in the spectral region (1000–3000 cm^{-1}). When extension of the low-wavenumber limit was necessary (below 1000 cm^{-1}), a ZnSe window was used. Au wire was used as the counter electrode, and a reversible hydrogen electrode (RHE) was used as the reference. Electrolyte solution of ethanol was prepared with Millipore water (18 MΩ cm) and analytical grade (Merck) chemicals. 0.1 M $HClO_4$ (Merck, Suprapur) was used as a supporting electrolyte. Before spectrochemical measurements, the solution was purged with pure nitrogen (U quality from L'air Liquide) and all the measurements were done at least three times with freshly prepared electrode at room temperature. In situ IR reflectance spectra in the wavenumber region 1000–3000 cm^{-1} were collected by a Fourier transform infrared spectrometer (Bruker IFS 66v) with an incidence angle of 65°. This instrument is equipped with nitrogen-cooled HgCdTe detector. The IR light beam passes entirely a chamber under vacuum before the observation of reflectance spectra of the electrode–electrolyte interface through the IR window (CaF_2/ZnSe) of a conventional thin layer spectroelectrochemical cell. This avoids recording parasitic spectra from the air atmosphere. Parallel polarized light was obtained from a BaF_2-supported AI grid polarizer. The cell potential was controlled using an LB 81 Wenking potentiostat and a Hi-Tech waveform generator, connected to a BD 90 XY recorder. The spectral resolution was 4 cm^{-1}. The reproducibility of the spectral acquisition was controlled by repeating each experiment at least three times, with freshly prepared electrodes. Data acquisition and processing were performed using a computer with OPUS 5.5 software (developed by Bruker). Using the Single Potential Alteration Infrared Reflectance Spectroscopy (SPAIRS) method, the electrode reflectivity RE_i was regularly recorded each 0.05 V during the first cyclic voltammogram (CV) scan rate at 1 mV s^{-1}. This method is suitable for detecting the exact potential at which product is formed. Each spectrum resulted from the co-addition of 128 interferograms. The data acquisition required 50 s, i.e. over 0.05 V steps from 0.05 to 1 V vs. RHE increased the potential. The results were displayed as $\Delta R/R = (RE_2 - RE_1)/RE_1 = -\Delta A$, where RE_1 is the reflectivity at potential E_1 and RE_2 the reflectivity at the potential E_2. For the calculation, E_1 can be taken at the initial potential of the CV; E_2 is some value along the CV. Within this definition, a negative band means the production of species at the sample potential and a positive band indicates the consumption of species at the electrode surface.

In this work, in order to detect the formation and the evolution of the adsorbed CO_L band, a series of SPAIR spectra was calculated using reference spectra at 0.9 V vs. RHE where CO totally oxidized [17]. To follow the appearance of CO_2, a reference spectrum was similarly recorded at 0.05 V vs. RHE, a potential at which CO_2 is absent from the solution.

3. Results and discussion

3.1. Physicochemical characterization of the catalysts

Since the Pt/C, $Pt_{90}Sn_{10}$/C and $Pt_{80}Sn_{10}M_{10}$/C (M = Ni, Co, Pd, Rh) catalysts used in this study are obtained by the same procedure as described in our previous papers [15,16], some information about their morphology, composition and structure are also collected from those papers (see Table 1). The atomic compositions of PtSn and PtSn based trimetallic catalysts were evaluated by energy dispersive X-ray microanalysis (EDX). It is found that the bulk elemental atomic compositions of the PtSn-based trimetallic catalysts were close to the nominal values, except for the Sn content in PtSn/C catalyst which was three times higher than the expected value. Transmission electron microscopy (TEM) analysis showed that nanoparticles are homogenously dispersed on the carbon surface in all catalyst. The average particle size was close to 3 nm, The X-ray diffractograms (XRD) revealed that the typical Pt fcc structure. The lattice parameter was also calculated in order to evaluate the level of alloying in the catalyst. PtSnNi/C catalyst showed a reduction in the Pt lattice parameter compared with Pt (3.911), which was perceived to be an improvement in Pt–Sn–Ni interaction. In contrast, the lattice parameter of PtSn/C and PtSnM/C (M = Co, Rh, Pd) catalysts was increased compared to that of Pt/C. This means that the level of alloying of these catalysts is lower than that of PtSnNi/C. The X-ray photon electron

Table 1
Physico-chemical paramaters of the prepared catalysts [15,16].

Catalyst	Nominal composition [at.%]	Atomic composition [at.%]	Surface composition [at.%]	Lattice parameter (Å)	Average crystallite size (nm)	Average TEM particle size (nm)
Pt/C				3.911	3.7	3.1
PtSn/C	90:10	72:28	69:31	3.917	6.1	2.9
PtSnNi/C	80:10:10	81:11:8	84:16:0	3.906	2.2	3.1
PtSnCo/C	80:10:10	77:13:10	83:17:0	3.938	2.1	3.2
PtSnPd/C	80:10:10	75:14:11	n.d.	3.917	4.4	n.d.
PtSnRh/C	80:10:10	86:7:7	76:24:0	3.923	2.2	2.8

spectroscopy (XPS) results showed that the particle surface of all catalysts were Sn-rich as compared to bulk composition, whereas for PtSnNi/C and PtSnCo/C catalysts were Pt-rich. As revealed from the binding energy, catalyst surface is mostly composed of oxidized states of Pt and Sn.

3.2. *In situ* FTIR measurements

Fig. 1 shows the linear sweep voltammograms of the carbon supported Pt, PtSn and PtSn-based trimetallic catalysts in 0.1 M $HClO_4$ + 0.1 M CH_3CH_2OH solution with a scan rate of 1 mV s^{-1}. Noticeably, two peaks appeared in the potential range of 0.05–1 V vs. RHE. The first peak at much lower potentials is more pronounced on carbon supported PtSn-based trimetallic catalysts compared to the Pt/C and $Pt_{90}Sn_{10}$/C. However, the addition of the third metal to the $Pt_{90}Sn_{10}$/C catalyst significantly promotes the catalytic activity with the low onset potential values for the oxidation of ethanol. Especially in the low potential range, $Pt_{80}Sn_{10}Co_{10}$/C catalyst shows the highest catalytic activity in comparison with the other trimetallic catalysts. Moreover, it has a broad plateau current between 0.5 and 0.7 V, which is probably due to its highly oxophilic nature. It seems that the accumulation of the adsorbed intermediates would be higher on this catalyst surface as a result of the slow kinetics of the ethanol oxidation reaction at a low scan rate.

Figs. 2 and 3 show the recorded SPAIR spectra on carbon supported Pt, PtSn and PtSn-based trimetallic electrodes during ethanol oxidation. The band between 2040 and 2060 cm^{-1} corresponding to the linearly adsorbed CO_L [18–21] which is disappeared on the electrodes surface at high potential for all electrodes. The electrode surface is readily poisoned with adsorbed CO as early as 0.1 V vs. RHE (see in Fig. 2b). Chang et al. [22] has suggested that the poisoning reaction is induced immediately with the beginning of the direct oxidation. This idea could explain the results of CO poisoning at very low potentials on the electrode surfaces through the fast ethanol oxidation pathway, which is related to the dissociative adsorption of ethanol. The bands at around 1274–1281 cm^{-1} and 933 cm^{-1}, which are related, respectively, to C—O stretching of acetic acid [23,24] and C—C—O asymmetric stretching of acetaldehyde [25], start at around 0.5 V (Fig. 2). Noticeably, the intensity of the band at 933 cm^{-1} is increased rapidly in the potential range of 0.6–0.8 V (Fig. 2), suggesting that the acetaldehyde oxidation may be promoted by coverage of the adsorbed OH species. However, this band intensity starts to decrease at higher potentials than 0.8 V. On the other hand, a band appears at around 1717–1723 cm^{-1}, which corresponds to the vibration C=O of the carbonyl groups of the acetaldehyde or acetic acid [26–29], but is perturbed by the water bending mode about 1640 cm^{-1} [30–32]. The consumption of ethanol begins from 0.5 to 0.6 V in the thin layer by the observation of the positive going bands at 1454 and 1045 cm^{-1} related to the O—H in-plane deformation and the C—O stretching vibration in ethanol [33]. The feature near 1368 cm^{-1} and 1402 cm^{-1} are associated with the C—H and C—O stretching mode of acetate [34,35], respectively. It should be noted that these bands appear after the formation of acetic acid. Moreover, a new IR band near 1604 cm^{-1} (Fig. 3g), possibly associated with the C=O stretching mode of adsorbed acetyl species [34,36–39].

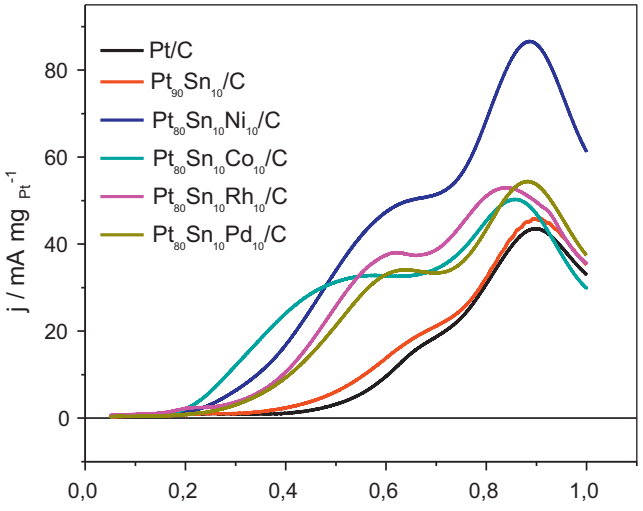

Fig. 1. Cyclic voltammograms of Pt/C, $Pt_{90}Sn_{10}$/C bimetallic and $Pt_{80}Sn_{10}M_{10}$/C (M = Ni, Co, Rh, Pd) trimetallic catalysts in 0.1 M $HClO_4$ + 0.1 M CH_3CH_2OH solution with a scan rate of 1 mV s^{-1} at 25 °C.

The obtained IR results on the $Pt_{80}Sn_{10}M_{10}$/C (M = Ni, Co, Rh, Pd) trimetallic electrodes is presented in Fig. 3. For all electrodes, the adsorbed CO_L formation is detected at low potential ca. 0.1 V vs. RHE and it is totally consumed above 0.7 V vs. RHE. Also, the formation of CO_2 (ca. 0.5 V vs. RHE) occurs at the same potential in comparison with Pt/C. This indicates that there should be other intermediates than CO_{ads} to be further oxidized to CO_2. Therefore, the addition of a second or of a third metal has not any remarkable effect on the potential for the formation of CO_2.

The CO band intensity and frequency on the catalyst surface can be explained by the nature of the catalyst and the effect of potential to the surface. On one side, the increase of CO stretching frequency with increasing positive potential is due to the increasing electric field at the interface, which is known as Stark effect [40,41]. On the other side, lateral interaction and chemical effects (competition for back bonding electrons) due to the surface coverage degree grows with adsorbed CO in function of the applied potential may cause a blue shift of the band centre [42]. The relationship between the surface electric field and the applied electrode potential is termed as "Stark tuning rate" (cm^{-1} V^{-1}). At low CO coverage (<0.13 ML), this value is found to be 45 cm^{-1} V^{-1} on a polycrystalline Pt electrode in 0.1 M $HClO_4$; however, at saturation coverage (~0.65 ML) decreased down to 30 cm^{-1} V^{-1} [43–48]. Potential dependence of the relative band intensities for CO_L (2040 cm^{-1}) and CO_2 (2345 cm^{-1}) species formed during ethanol oxidation on Pt/C, $Pt_{90}Sn_{10}$/C and $Pt_{80}Sn_{10}M_{10}$/C (M = Ni, Co, Rh, Pd) electrodes are presented in Fig. 4. In addition, the potential dependent CO_L band centre frequencies are plotted in the inset of Fig. 4. The evolution of CO_2 band intensity as a function of potential provides evidence for different reaction mechanism on Pt/C and $Pt_{90}Sn_{10}$/C and $Pt_{80}Sn_{10}M_{10}$/C (M = Ni, Co, Rh, Pd) trimetallic

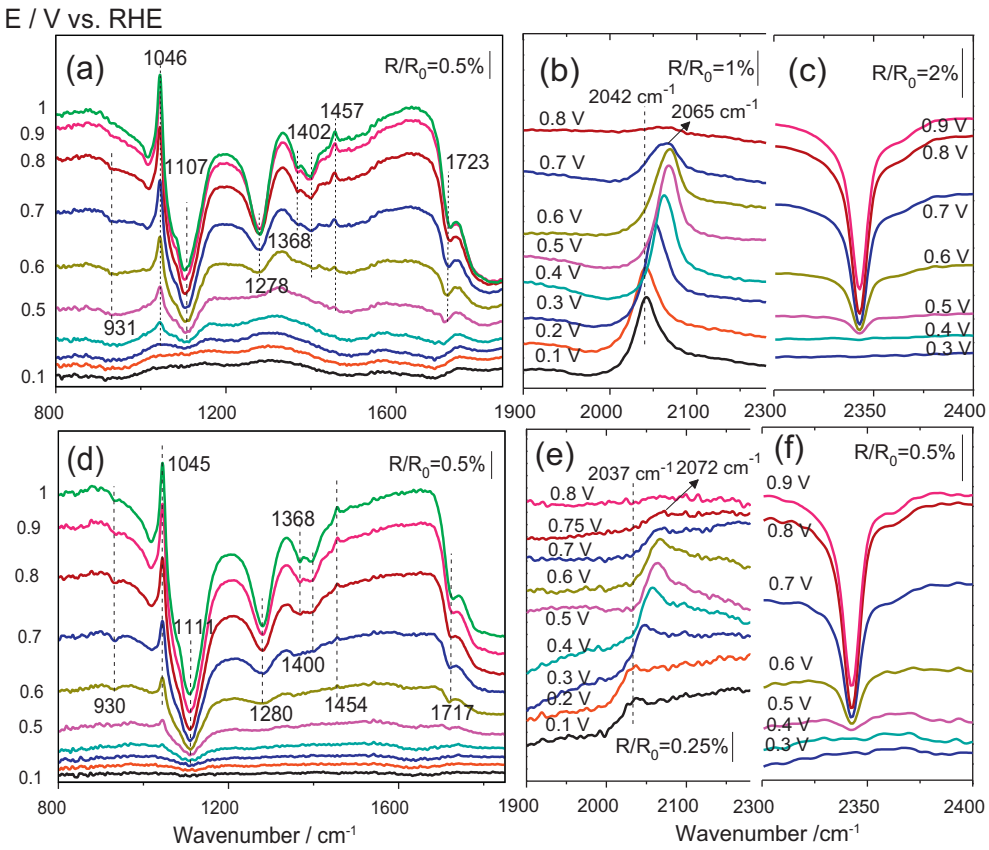

Fig. 2. SPAIR spectra obtained on Pt/C and $Pt_{90}Sn_{10}$/C electrodes in 0.1 M CH_3CH_2OH + 0.1 M $HClO_4$. A flat ZnSe window was used for acetaldehyde (933 cm^{-1}) and acetic acid bands (1280 cm^{-1}) (a, d) and a prismatic CaF_2 window for CO (2050 cm^{-1}), CO_2 (2340 cm^{-1}) bands (b, c, e, f). The reference spectrum was collected at 0.05 V vs. RHE and the sample spectra were taken after applying potential steps towards more positive potentials. The CO region (b, e) was calculated with a reference spectrum taken at 0.9 V vs. RHE (after complete CO oxidation). The CO_2 region (c, f) was calculated with a reference spectrum taken at 0.05 V vs. RHE.

electrodes. For all electrodes studied in this work, CO_2 appears at ca. 0.5 V vs. RHE according to the band at 2345 cm^{-1}, which the intensity increases with the potential. The linearly adsorbed CO_L is observed as early as 0.1 V vs. RHE and is strongly present to the electrode surface according to the band between 2020 and 2050 cm^{-1}. For the Pt/C electrode, the CO vibrational Stark tuning rate is found to be around 89 cm^{-1} V^{-1} in the inset of Fig. 4a. Furthermore, the stretching frequency of adsorbed CO_L varies linearly in the potential range of 0.2–0.5 V vs. RHE. Above ca. 0.5 V vs. RHE, where CO_L starts being oxidized, the CO_L band centre frequency decreases. This can be interpreted as a red-shift. The decreasing of the CO_L band (2067 cm^{-1}) at higher potentials than 0.5 V is due to the formation of CO_2 (2345 cm^{-1}). A parallel increase of the band centre frequency and coverage of CO is observed up to a potential of about 0.5 V vs. RHE (see in Fig. 4a–c). At higher potential than 0.5 V, the effect of an increasing electric field (increasing positive charge on the metal) should be an increase of the separation of charges in the CO which is oriented with the negative part (oxygen atoms) towards the metal. This would result in an enlargement of the C—O bond, i.e. a downward shift of the band centre with increasing positive potential should be expected. For all that, $Pt_{80}Sn_{10}Ni_{10}$/C electrode surface (Fig. 4c), at potentials higher than 0.5 V, the CO_L band centre frequency is remained constant to decreasing CO coverage or increasing electric field, after slight red shift is observed. This indicates that adsorbed species govern the behaviour of the band centres. Interestingly, the adsorption of ethanol on $Pt_{80}Sn_{10}Co_{10}$/C electrode seems to reach the saturation as indicated by the constant CO_L band intensity up to a potential of about 0.4 V (Fig. 4d). In the potential range between 0.1 and 0.4 V, the Stark tuning rate is 51 cm^{-1} V^{-1}. Noticeably, this value is considerably lower than Pt/C (89 cm^{-1} V^{-1}), $Pt_{90}Sn_{10}$/C (91 cm^{-1} V^{-1}) and $Pt_{80}Sn_{10}Ni_{10}$/C (84 cm^{-1} V^{-1}) electrodes, suggesting that the higher CO coverage on the surface of $Pt_{80}Sn_{10}Co_{10}$/C electrode in accordance with the slow kinetics of adsorbed CO species at low potentials (Fig. 1). As pointed out before, all electrode surfaces completely poisoned already at 0.1 V vs. RHE and only linear bonded CO_L can be identified as the poisoning intermediate at the initial stage. Besides linearly bonded CO_L, a small band at 1850 cm^{-1}, which can be assigned to bridge bonded CO_B [18–21] is also observed on $Pt_{80}Sn_{10}Rh_{10}$/C electrode (Fig. 4e). The intensity of this band diminishes until ca. 0.3 V vs. RHE in which the coverage of CO_L increases. This provides an evidence of the conversion of CO_B to CO_L at potentials lower than 0.3 V. This phenomenon has also been reported for CO adsorbed on Pt(1 0 0) by Kitamura et al. [49], who pointed out that the conversion, is reversible with the potential.

It has been shown by some researchers [50–53] that the electronic state of metal supported catalysts also affects the adsorption of CO by a blue shift of the vibrational frequency of C—O. In this sense, the higher frequency of CO band can be assigned to completely oxidized to Pt particles and the lower frequency of CO band represented by the lower oxidation states of Pt. Noticeably, we observed that the relative shift of the C—O vibrational frequency as high as 35 cm^{-1} (from 2037 to 2072 cm^{-1}) for $Pt_{90}Sn_{10}$/C and as low as 16 cm^{-1} (from 2038 to 2054 cm^{-1}) for $Pt_{80}Sn_{10}Co_{10}$/C (Figs. 2 and 3). Therefore, we would expect that the electronic state of Pt is mostly oxidized in $Pt_{90}Sn_{10}$/C; however, in the case of $Pt_{80}Sn_{10}Co_{10}$/C both reduced and oxidized Pt could be present. This assumption is verified by surface characterization from our previous XPS study [15,16].

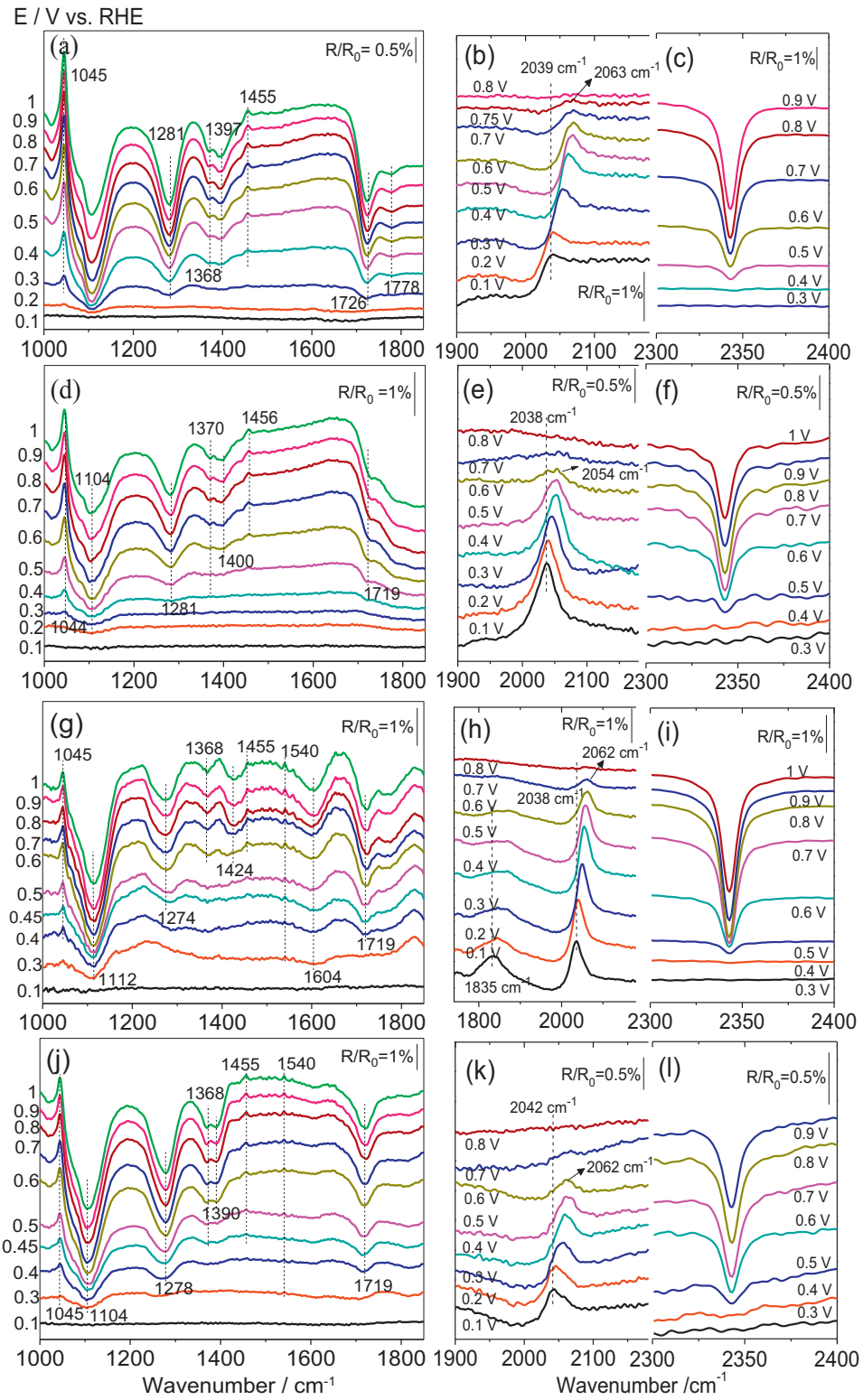

Fig. 3. SPAIR spectra obtained on $Pt_{80}Sn_{10}Ni_{10}/C$ (a–c), $Pt_{80}Sn_{10}Co_{10}/C$ (d–f), $Pt_{80}Sn_{10}Rh_{10}/C$ (g–i) and $Pt_{80}Sn_{10}Pd_{10}/C$ (j–l) electrodes in 0.1 M CH_3CH_2OH + 0.1 M $HClO_4$. A prismatic CaF_2 window was used for acetic acid bands (1280 cm^{-1}) (a, d, g, j) and for CO (2050 cm^{-1}) (b, e, h, k), CO_2 (2340 cm^{-1}) (c, f, i, l) bands. The spectra were obtained and computed as described in Fig. 2.

The band relative to the production of CO_2 during ethanol oxidation on different plurimetallic electrodes in comparison with Pt/C is presented in the Fig. 5a. Pt/C, $Pt_{80}Sn_{10}Ni_{10}/C$ and $Pt_{80}Sn_{10}Rh_{10}/C$ electrodes showed a better performance than $Pt_{90}Sn_{10}/C$, $Pt_{80}Sn_{10}Co_{10}/C$ and $Pt_{80}Sn_{10}Pd_{10}/C$ electrodes for production of CO_2 during the ethanol oxidation. A low level of CO_2 formation indicates that these catalysts have a poor activity towards the scission of the C—C bond. It is noteworthy that the pathway forming CO_2 is favoured by the presence of Ni and Rh. Therefore, the addition of Ni or Rh to $Pt_{90}Sn_{10}/C$ electrode would

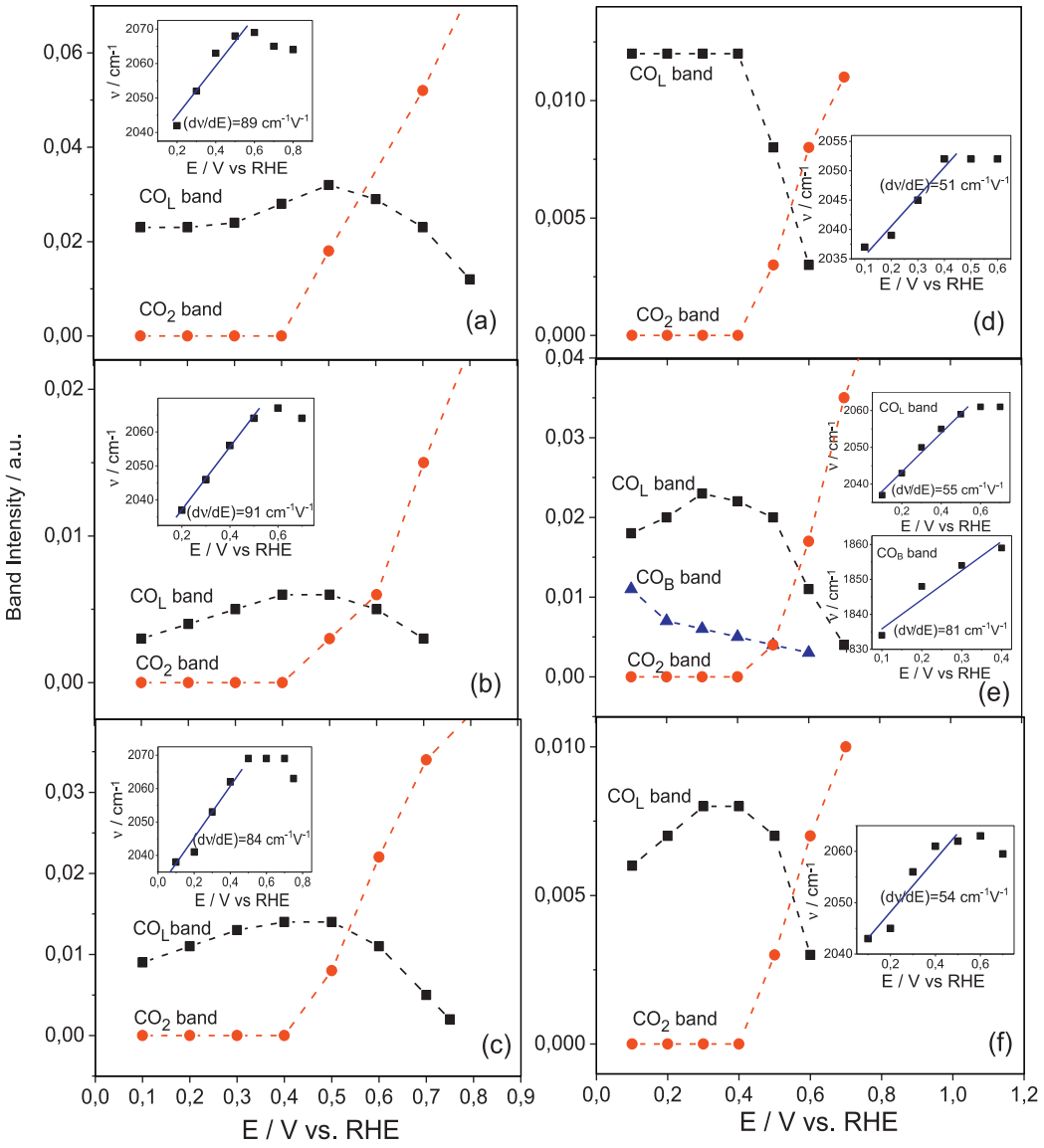

Fig. 4. Potential dependence of the band intensities for CO_2 (2341 cm^{-1}), CO_L (2050 cm^{-1}) and for CO_B (1850 cm^{-1}) formed during the first anodic polarization of Pt/C (a), $Pt_{90}Sn_{10}$/C (b), $Pt_{80}Sn_{10}Ni_{10}$/C (c), $Pt_{80}Sn_{10}Co_{10}$/C (d), $Pt_{80}Sn_{10}Rh_{10}$/C (e) and $Pt_{80}Sn_{10}Pd_{10}$/C (f) electrodes in 0.1 M CH_3CH_2OH + 0.1 M $HClO_4$ (from spectra in Figs. 2 and 3). Insets: corresponding the potential dependence of the band centre frequency for linearly bonded CO_L and bridge bonded CO_B.

enhance the activity and facilitate the cleavage of the C—C bond. Nevertheless, the relative quantity of produced CO_2 remains superior on the Pt electrode. The evolution of the CO_L band intensity according to the potential for different plurimetallic electrodes compared with Pt/C is presented in Fig. 5b. It appears that the $Pt_{90}Sn_{10}$/C and $Pt_{80}Sn_{10}Pd_{10}$/C electrodes are the most weakly poisoned by the linearly bonded CO_L. In fact, the band intensity increases until 0.4 V vs. RHE, but still, remains inferior in comparison with the other electrodes. Pt electrode presents a higher poisoning by CO_L in comparison with plurimetallic electrodes in the whole range of potential considered. $Pt_{80}Sn_{10}Rh_{10}$/C and $Pt_{80}Sn_{10}Ni_{10}$/C electrodes show an intermediate poisoning according to the observed intensities. Interestingly, the CO_L superficial concentration remains constant until 0.4 V vs. RHE, and then linearly bonded CO_L begins to oxidize significantly on $Pt_{80}Sn_{10}Co_{10}$/C electrode. Acetic acid production shows a steep increase on the $Pt_{80}Sn_{10}Ni_{10}$/C and $Pt_{80}Sn_{10}Pd_{10}$/C electrodes (see Fig. 5c). Although the CO_2 is the lowest yields of ethanol oxidation on $Pt_{80}Sn_{10}Pd_{10}$/C electrode, the main effect of Pd is reflected in the increased production of acetic acid.

3.2.1. *Mechanism of adsorption and oxidation of ethanol on Pt/C electrode*

The results obtained from in situ FTIR spectroscopy measurements as discussed above, it is likely that a fast ethanol oxidation pathway through the adsorbed acetaldehyde and/or acetyl species on Pt sites, leading to the adsorbed CO and residual CH_x species:

$$Pt(CH_3CH_2OH)_{ads} \rightarrow Pt(CH_3CO)_{ads} + 3H^+3e^- \rightarrow Pt(CO)_{ads} + Pt{-}CH_3 \quad (1)$$

Consequently, the adsorbed CO on Pt is observed at very low potential. On the other hand, the oxygenated species formed on the Pt electrode at higher potentials than 0.5 V vs. RHE, which allow the oxidation of the adsorbed CO to CO_2.

$$H_2O + Pt \rightarrow Pt(OH)_{ads} + H^+ + e^- \quad (2)$$

$$Pt(OH)_{ads} + Pt(CO)_{ads} \rightarrow Pt + CO_2 + H^+ + e^- \quad (3)$$

The band at 2345 cm^{-1} in the SPAIRS spectrum confirms the formation of CO_2 at higher potentials than 0.5 V. Furthermore, the

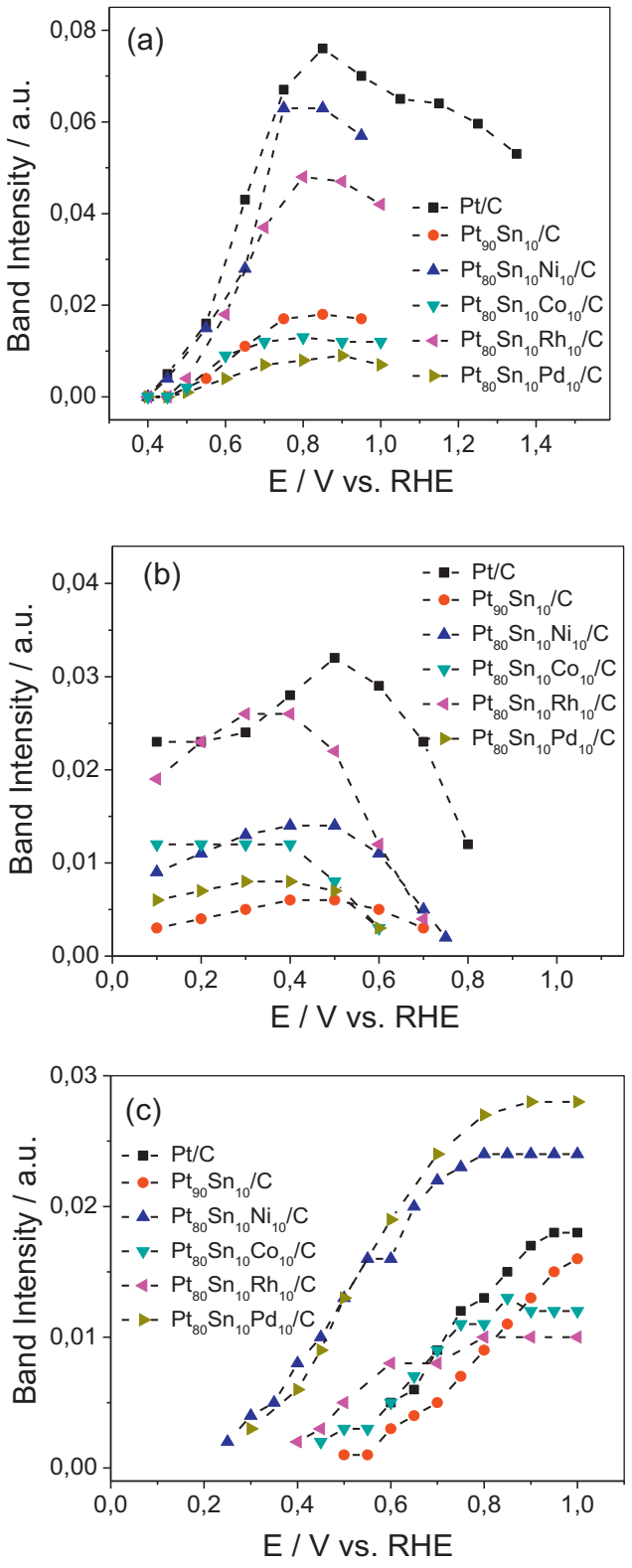

Fig. 5. Comparison of the potential dependence of the band intensities for CO_2 (2345 cm^{-1}) (a) and CO_L (2040 cm^{-1}) (b) for CH_3COOH (1280 cm^{-1}) (c) obtained on Pt/C, $Pt_{90}Sn_{10}$/C, and $Pt_{80}Sn_{10}M_{10}$/C (M = Ni, Co, Rh, Pd) electrodes in 0.1 M CH_3CH_2OH + 0.1 M $HClO_4$ (from spectra in Figs. 2 and 3).

SPAIRS technique allows us to observe the partial ethanol oxidation to acetaldehyde and acetic acid for potentials higher than 0.5 V on Pt/C electrode according to Eqs. (4) and (5).

$$Pt(CH_3CH_2OH)_{ads} \rightarrow Pt(CH_3CHO)_{ads} + 2H^+ + 2e^- \quad (4)$$

$$Pt(CH_3CHO)_{ads} + Pt(OH)_{ads} \rightarrow Pt(CH_3COOH)_{ads} + Pt + H^+ + e^- \quad (5)$$

3.2.2. Mechanism of adsorption and oxidation of ethanol on PtSn/C electrode

On the $Pt_{90}Sn_{10}$/C electrode, adsorbed ethanol is dissociated giving rise to the formation of acetaldehyde ($E > 0.5$ V vs. RHE), which is confirmed by the negative-going band at 933 cm^{-1} (Fig. 2d). The electronic influence of Sn favours the weak adsorption of acetaldehyde on the sites of Pt leading to desorption without further oxidation:

$$Pt(CH_3CHO)_{ads} \rightarrow Pt(CH_3CHO)_{sol} + Pt \quad (6)$$

This assumption is supported by our recent FTIR study [54], showing the low conversion of acetaldehyde to CO_2 in the presence of Sn. The formation of CO_2 was similar to the Pt/C electrode according to Eqs. (1)–(3). However, Sn provides oxygenated species due to the activation of the water at low potentials, which provides the lower oxidation potential of the adsorbed CO_{ads} to CO_2 and weakly adsorbed acetaldehyde to acetic acid comparing to Pt sites:

$$H_2O + Sn \rightarrow Sn(OH)_{ads} + H^+ + e^- \quad (7)$$

$$Pt(OH)_{ads} + Sn(OH)_{ads} \rightarrow Pt + Sn + CO_2 + H^+ + e^- \quad (8)$$

$$Pt(CH_3CHO)_{ads} + Sn(OH)_{ads} \rightarrow Pt + Sn + CH_3COOH + H^+ + e^- \quad (9)$$

The effect of Sn on $Pt_{90}Sn_{10}$/C catalyst appears to limit the production of CH_3CHO and CO_2 but increase the selectivity to CH_3COOH, concurring with the literature [11,54–58].

3.2.3. Mechanism of adsorption and oxidation of ethanol on PtSn-based trimetallic electrodes

There is a remarkable similarity between $Pt_{80}Sn_{10}Ni_{10}$/C and $Pt_{80}Sn_{10}Pd_{10}$/C electrodes based on the mechanism of dissociative adsorption of ethanol. SPAIRS results showed that ethanol is oxidized to acetic acid at very low potentials on these electrodes ($E < 0.3$ V vs. RHE).

In a direct oxidation pathway, adsorbed ethanol is oxidized to the acetic acid according to Eq. (10):

$$Pt(CH_3CH_2OH)_{ads} + H_2O \rightarrow Pt + Sn + CH_3COOH + 4H^+ + 4e^- \quad (10)$$

Therefore, it would appear that the adsorbed water on the surface plays an important role for this pathway. Li and Iglesia [59] have found that the water increases the direct oxidation of ethanol to acetic acid on dispersed Mo–V–Nb mixed oxides by inhibiting the formation of acetaldehyde. Along the same lines, Mederios et al. [60] have investigated the role of water in the oxidation of ethanol to acetic acid on Sn–Mo–O catalysts by FTIR spectroscopy. In their study of ethanol oxidation, they proposed that the presence water in the stream induces desorption of adsorbed species which prevents formation of by products. Water enhances the selectivity to acetic acid but decreases the ethanol conversion through hydroxyl groups on the surface active sites. In our recent study [54], we found that the acetyl species is obviously favoured on the $Pt_{80}Sn_{10}Pd_{10}$/C at very low potential during the oxidation

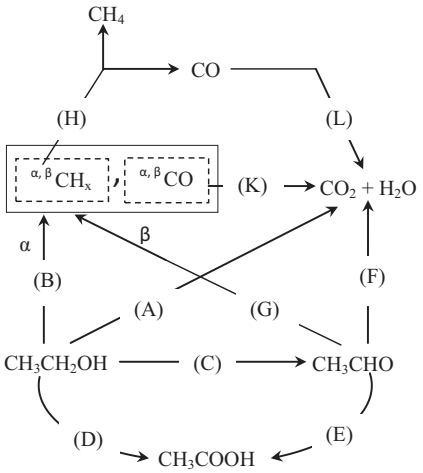

Fig. 6. A general scheme for the mechanism of ethanol oxidation on carbon supported Pt, PtSn and PtSn-based trimetallic electrodes.

of acetaldehyde. In this sense, we can expect that the adsorbed acetyl species is more easily oxidized to acetic acid through surface hydroxyl species on the $Pt_{80}Sn_{10}Pd_{10}/C$ electrode compared to the other PtSn-based trimetallic electrodes. In our forthcoming publication, which includes the FTIR study of the adsorption and oxidation of acetic acid, both $Pt_{80}Sn_{10}Pd_{10}/C$ and $Pt_{80}Sn_{10}Ni_{10}/C$ showed a relative sharp band at around 3200 cm^{-1} in the OH stretching frequency region. It would seem that surface charge density of these electrodes is strongly connected to the bonding scheme of adsorbed water. Suppose that a relative negative charge on the $Pt_{80}Sn_{10}Pd_{10}/C$ and $Pt_{80}Sn_{10}Ni_{10}/C$ electrodes is the cause of weakened the O—H bond easily compared to other PtSn-based trimetallic electrodes.

Besides a high selectivity towards acetic acid formation, $Pt_{80}Sn_{10}Pd_{10}/C$ electrode exhibited the lowest ethanol conversion to CO_2. From SPAIRS results, a small amount of CO_2 formed on $Pt_{80}Sn_{10}Pd_{10}/C$ electrode relative to the other electrodes during the oxidation of ethanol. This can be related to the quite weak adsorption of CO on the electrode surface. In contrast, $Pt_{80}Sn_{10}Ni_{10}/C$ and $Pt_{80}Sn_{10}Rh_{10}/C$ electrodes provide a high conversion of ethanol to CO_2. This suggests that Ni or Rh can promote the breaking C—C bond. A high CO_2 selectivity of Rh over noble metals (Pt, Ru, and Pd) has also been proposed by several authors [61–65].

According to the in situ IR results, a general scheme for the mechanism of the partial oxidation of ethanol on carbon supported Pt, PtSn and PtSn-based trimetallic electrodes can be summarized in Fig. 6. Based on this mechanism, ethanol is dissociatively adsorbed giving rise to CH_3CHO species (step C), which can be decomposed either producing CH_x and CO or dehydrogenated (step G). In the case of $Pt_{80}Sn_{10}Ni_{10}/C$ and $Pt_{80}Sn_{10}Pd_{10}/C$ electrodes, ethanol is oxidized to CH_3COOH either directly (step D) or via CH_3CHO route (steps C and E) at very low potentials ($E \sim 0.2$–0.3 V vs. RHE). On the other hand, on $Pt_{90}Sn_{10}/C$ electrode, the formation of weakly adsorbed CH_3CHO is oxidized to CH_3COOH (step E), however, a significant amount desorbed from the surface to the solution. The oxidation of ethanol to CO_2 could involve two different steps either via CH_3CHO (steps C and F) or via CH_x and CO intermediates (steps B and K).

4. Conclusions

In situ FTIR spectroscopy studies showed that the Pt/C, $Pt_{80}Sn_{10}Ni_{10}/C$ and $Pt_{80}Sn_{10}Rh_{10}/C$ catalysts showed a better performance than $Pt_{90}Sn_{10}/C$, $Pt_{80}Sn_{10}Co_{10}/C$ and $Pt_{80}Sn_{10}Pd_{10}/C$ catalysts for oxidizing ethanol to CO_2. We can conclude that the presence of Ni or Rh in the PtSn catalysts lead to the cleavage of the C—C bond in ethanol, and the oxidation reaction pathways on $Pt_{90}Sn_{10}/C$, $Pt_{80}Sn_{10}Co_{10}/C$ and $Pt_{80}Sn_{10}Pd_{10}/C$ catalysts favour the formation of adsorbed intermediates. On the other hand, the addition of Ni or Pd to PtSn directly favours the formation of acetic acid at low potential. In the case of Pt/C and $Pt_{90}Sn_{10}/C$ catalysts, acetic acid detected at higher potentials than that of the trimetallic catalysts.

Acknowledgments

This work was carried out within the framework of a bilateral cooperation programme between Istanbul Technical University (Turkey) and Université de Poitiers (France). S.B. thanks Bourse du Governement Français (Contract #20064739) for support.

References

[1] J. Willsau, J. Heitbaum, Journal of Electroanalytical Chemistry 194 (1985) 27–35.
[2] T. Iwasita, E. Pastor, Electrochimica Acta 39 (1994) 531–537.
[3] G.A. Camara, T. Iwasita, Journal of Electroanalytical Chemistry 578 (2005) 315–321.
[4] S.C. Chang, L.W.H. Leung, M.J. Weaver, Journal of Physical Chemistry 94 (1990) 6013–6021.
[5] H. Wang, Z. Jusys, R.J. Behm, Journal of Physical Chemistry B 108 (2004) 19413–19424.
[6] U. Schmiemann, U. Muller, H. Baltruschat, Electrochimica Acta 40 (1995) 99–107.
[7] Q. Wang, G.Q. Sun, L.H. Jiang, Q. Xin, S.G. Sun, Y.X. Jiang, Physical Chemistry Chemical Physics 9 (2007) 2686–2696.
[8] F. Vigier, C. Coutanceau, F. Hahn, E.M. Belgsir, C. Lamy, Journal of Electroanalytical Chemistry 563 (2004) 81–89.
[9] J.P.I. De Souza, D.L. Queiroz, K. Bergamaski, E.R. Gonzalez, F.C. Nart, Journal of Physical Chemistry B 106 (2002) 9825–9830.
[10] E. Antolini, Journal of Power Sources 170 (2007) 1–12.
[11] S. Rousseau, C. Coutanceau, C. Lamy, J.-M. Léger, Journal of Power Sources 158 (2006) 18–24.
[12] J. Ribeiro, D.M. dos Anjos, K.B. Kokoh, C. Coutanceau, J.M. Léger, P. Olivi, A.R. de Andrade, G. Tremiliosi-Filho, Electrochimica Acta 52 (2007) 6997–7006.
[13] M. Zhu, G. Sun, S. Yan, H. Li, Q. Xin, Energy & Fuels 23 (2009) 403–407.
[14] H. Bönnemann, W. Brijoux, Active Metals: Preparation, Characterization, Applications, Catalytic Active Metal Powders and Colloids, VCH, Weinheim, Germany, 1995, pp. 339–378.
[15] S. Beyhan, J.M. Léger, F. Kadırgan, Applied Catalysis B: Environmental 130 (2013) 305–313.
[16] S. Beyhan, C. Coutanceau, J.M. Léger, T.W. Napporn, F. Kadırgan, International Journal of Hydrogen Energy 38 (2013) 6830–6841.
[17] F. Maillard, F. Gloaguen, F. Hahn, J.M. Léger, Fuel Cells 2 (2002) 143–152.
[18] B. Beden, C. Lamy, A. Bewick, K. Kunimatsu, Journal of Electroanalytical Chemistry 121 (1981) 343.
[19] K. Kunimatsu, Journal of Electroanalytical Chemistry 140 (1982) 205.
[20] B. Beden, F. Hahn, S. Juanto, C. Lamy, J.-M. Léger, Journal of Electroanalytical Chemistry 225 (1987) 215.
[21] B. Beden, A. Bewick, K. Kunimatsu, C. Lamy, Journal of Electroanalytical Chemistry 142 (1982) 345.
[22] S.C. Chang, L.W.H. Leung, M.J. Weaver, Surface Science 265 (1992) 81–94.
[23] L.-W.H. Leung, S.-C. Chang, M.J. Weaver, Journal of Physical Chemistry 92 (1988) 4019.
[24] D.S. Corrigan, E.K. Krauskopf, L.M. Rice, A. Wieckowski, M.J. Weaver, Journal of Physical Chemistry 98 (1988) 1596.
[25] P. Gao, S.-C. Chang, Z. Zhou, M.J. Weaver, Journal of Electroanalytical Chemistry 272 (1989) 161.
[26] T. Iwasita, E. Pastor, Electrochimica Acta 39 (1994) 531.
[27] S.C. Chang, L.W. Leung, M.J. Weaver, Journal of Physical Chemistry 94 (1990) 6013.
[28] T. Iwasita, B. Rasch, E. Cattaneo, W. Vielstich, Electrochimica Acta 34 (1989) 1073.
[29] J.M. Perez, B. Beden, F. Hahn, A. Aldaz, C. Lamy, Journal of Electroanalytical Chemistry 262 (1989) 251.
[30] S.D. Ross, Inorganic Infrared and Raman Spectra, McGraw Hill, London, 1972.
[31] B.A. Sexton, Surface Science 94 (1980) 435.
[32] B. Rasch, T. Iwasita, Electrochimica Acta 35 (1990) 989.
[33] J.G. Wu, Modern Fourier Transform Infrared Spectroscopy Techniques and their Applications, Scientific and Technical Document Publishing House, Beijing, 1994.
[34] A. Rodes, E. Pastor, T. Iwasita, Journal of Electroanalytical Chemistry 376 (1994) 109–118.
[35] L.-W.H. Leung, S.-C. Chang, M. Weaver, Journal of Electroanalytical Chemistry 266 (1989) 317.
[36] M.H. Shao, R.R. Adzic, Electrochimica Acta 50 (2005) 2415–2422.

[37] M. Heinen, Z. Jusys, R.J. Behm, Journal of Physical Chemistry C 114 (2010) 9850–9864.
[38] J.L. Davis, M.A. Barteau, Journal of the American Chemical Society 111 (1989) 1782–1792.
[39] R. Shekhar, M.A. Barteau, R.V. Plank, J.M. Vohs, Journal of Physical Chemistry B 101 (1997) 7939–7951.
[40] D. Lambert, Electrochimica Acta 41 (1996) 623–630.
[41] F.C. Nart, T. Iwasita, Electrochimica Acta 41 (1996) 631–636.
[42] F.M. Hoffmann, Surface Science Reports 3 (1983) 107.
[43] S.-C. Chang, M.J. Weaver, Surface Science 238 (1990) 142.
[44] S.-C. Chang, M.J. Weaver, Journal of Physical Chemistry 92 (1990) 4582.
[45] J.W. Russell, M. Severson, K. Scanlon, J. Overend, A. Bewick, Journal of Physical Chemistry 87 (1983) 293–297.
[46] K. Kunimatsu, W.G. Golden, H. Seki, M.R. Philpott, Langmuir 1 (1985) 245–250.
[47] K. Kunimatsu, K. Shimazu, H. Kita, Journal of Electroanalytical Chemistry 256 (1988) 371–385.
[48] J. Lu, A. Bewick, Journal of Electroanalytical Chemistry 270 (1989) 225–235.
[49] F. Kitamura, M. Takahashi, M. Ito, Surface Science 223 (1989) 493–508.
[50] R.K. Herz, E.J. Shinouskis, Applied Surface Science 19 (1984) 373–397.
[51] Z. Zhang, A. Kladi, X.E. Verykios, Journal of Physical Chemistry 98 (1994) 6804–6811.
[52] Z. Zhang, A. Kladi, X.E. Verykios, Journal of Catalysis 156 (1995) 37–50.
[53] C. Elmasides, D.I. Kondarides, S.G. Neophytides, X.E. Verykios, Studies in Surface Science and Catalysis 130 (2000) 3083–3088.
[54] S. Beyhan, J.M. Léger, F. Kadırgan, Journal of Power Sources 242 (2013) 503–509.
[55] F. Vigier, C. Coutanceau, A. Perrard, E.M. Belgsir, C. Lamy, Journal of Applied Electrochemistry 34 (2004) 439–460.
[56] F. Vigier, S. Rousseau, C. Coutanceau, J.-M. Léger, C. Lamy, Topics in Catalysis 40 (2006) 111–121.
[57] E. Antolini, Applied Catalysis B 74 (2007) 337–350.
[58] G. Wu, R. Swaidan, G.F. Cui, Journal of Power Sources 172 (2007) 180–188.
[59] X. Li, E. Iglesia, Chemistry – A European Journal 13 (2007) 9324–9330.
[60] P.R.S. Medeiros, J.G. Eon, L.G. Appel, Catalysis Letters 69 (2000) 79–82.
[61] J.P. Breen, R. Burch, H.M. Coleman, Applied Catalysis B 39 (2002) 65–74.
[62] F. Frusteri, S. Freni, L. Spadaro, V. Chiodo, G. Bonura, S. Donato, Catalysis Communications 5 (2004) 611–615.
[63] D.K. Liguras, D.I. Kondarides, X.E. Verykios, Applied Catalysis B 43 (2003) 345–354.
[64] J.R. Salge, G.A. Deluga, L.D. Schmidt, Journal of Catalysis 235 (2005) 69–78.
[65] P.Y. Sheng, H. Idriss, Journal of Vacuum Science & Technology A 22 (2004) 1652–1658.